# Three-dimensional thermoelastohydrodynamic analysis of pivoted pad thrust bearings
# Part 2: application of theory and comparison with experiments

**Y M H Ali El-Saie,** BSc(Eng), PhD, DIC and **R T Fenner,** PhD, DSc(Eng), CEng, FIMechE, DIC
Department of Mechanical Engineering, Imperial College of Science and Technology, Exhibition Road, London SW7

*In Part 1, a computational method was described for predicting the performance of pivoted pad thrust bearings. In this second part, computed results are compared with experimental data. Three test cases are considered, which cover the range of bearing sizes normally encountered in practice, from a 150 mm diameter laboratory scale experiment through the main propulsion thrust bearings of a destroyer to a 3 m diameter bearing. Generally good agreement is obtained for both temperatures and film thicknesses.*

## 1 INTRODUCTION

Part 1 dealt with the numerical modelling of tilting pad thrust bearings. While individual parts of the model can be tested against, for example, relatively simple cases for which analytical or other numerical solutions exist, the validity of the model as a whole can only be effectively verified by comparison with experimental results.

Three test cases have been chosen. The first concerns a large tilting thrust bearing of the type used for large hydroelectric generators. The second is medium size, typical of marine thrust bearings. The third is a small bearing size, typical of the high angular velocity small rotor applications. These three test cases span across the tilting thrust bearing size range and therefore present good checks for the model used.

## 2 CASE 1—LARGE THRUST BEARING

The experimental results have been accessed through an internal company report **(1)**. The basic bearing specifications are listed in Table 1. The bearing is composed of ten equally spaced pads. The basic pad geometry is shown in Fig. 1. The pads are individually supported by centrally relieved buttons. They were designed to control the amount of pad deflection and to provide some flexibility in the bearing, thus equalizing the individual loads on the pads. Extensive temperature measurements in the pads were carried out. The thermocouple installation and positions for all ten pads of the bearing are shown in Fig. 1. The thermocouples along the inlet edges of the pad were very close to the working surface whereas the remaining thermocouples were approximately 13 mm from the surface. At four positions on one of the pads, thermocouples were installed on the back face as well as 13 mm from the working surface. By assuming a parabolic law for the temperature profile across the pad thickness, it has been possible to obtain values for the surface temperatures.

During start-up, the bearing is hydraulically jacked via a jacking oil groove in the pad face (see Fig. 1). During operation, the jacking oil supply is shut off and a pressure gauge installed to measure the oil film pressure immediately in front of the thrust pad in the jacking pipeline, with the jacking pump switched off. The oil bath temperature was kept constant at 48°C.

### 2.1 Numerical model

Since the pads are not centrally pivoted, the grid spacings were varied to accommodate the support shape (a circular ring) as closely as possible. Figure 2 shows a plan of the pad with the grid superimposed. Also shown are the support nodes chosen as the nodes closest to the ring support. The boundary conditions used for the pad deflection are also shown. These include free pad edges and corners. At the support positions, no allowance has been made for the pivot elasticity. At the corners, the shear forces produced by the torsional moments

**Table 1** Bearing data for case 1

| | |
|---|---|
| Pad angle | 29.5 degrees |
| Inner radius ($R_i$) | 0.7493 m |
| Outer radius ($R_o$) | 1.4732 m |
| Number of pads | 10 |
| Pad thickness—minimum | 0.0762 m |
| —maximum | 0.2032 m |
| Pivot position | |
| radius | 1.151 m |
| circumferential at O | 16.05 degrees |
| Angular velocity | 85.7 r/min |
| Oil viscosity | 625 SSU at 100°F |
| | 169 SSU at 150°F (interpolated) |
| | 210 SSU at 210°F (interpolated) |
| Bath temperature | 48°C |
| Pad material | Steel |
| (Values constant throughout) | |
| Oil density | 899 kg/m$^3$ |
| Oil conductivity | 0.15 J/m s°C |
| Oil specific heat | 1880 J/kg s°C |
| Steel conductivity | 45 J/kg s°C |
| Steel coefficient of linear expansion | $1.1 \times 10^{-5}$ |
| Poisson ratio | 0.3 |

*The MS was received on 3 February 1987 and was accepted for publication on 4 September 1987.*

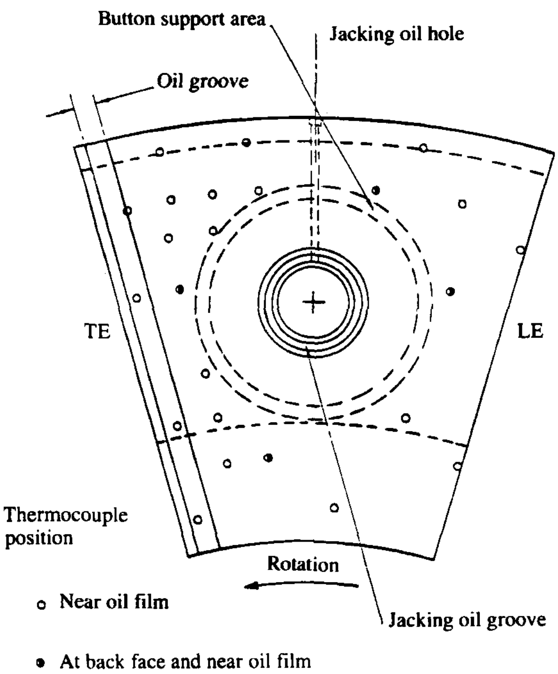


**Fig. 1** Pad geometry (case 1)

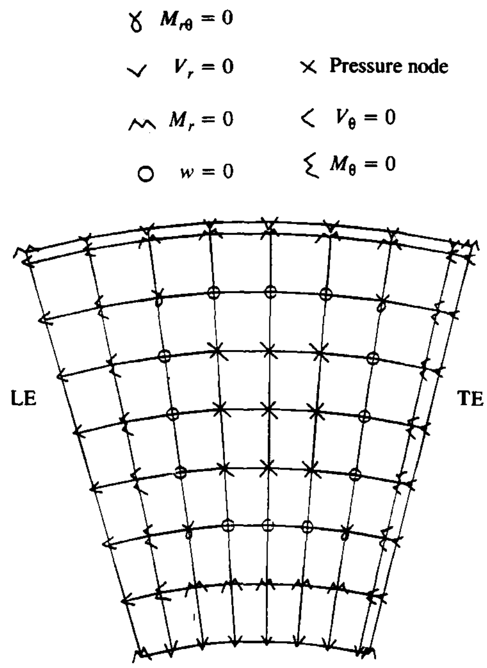


**Fig. 2** The grid and boundary conditions for deflection (case 1)

($M_{xy}$, $M_{yx}$) are additive (**2**). A net force ( $= 2M_{xy}$) is thus produced at the corners and must be set to zero in a free corner case.

In order to estimate the surface heat-transfer coefficient at the back face of the pads, the oil bath temperature has been used as the 'free' stream temperature. Thus,

$$\alpha(T_{\text{bath}} - T_{\text{surface}}) = k\left(\frac{T_{\text{surface}} - T_{\text{pad}}}{\text{depth}}\right)$$

where

$T_{\text{surface}}$ = back face temperature
$T_{\text{pad}}$ = temperature at a location near the pad working surface
depth = distance from the back face to the location of $T_{\text{pad}}$
$k$ = conductivity of the pad
$\alpha$ = surface heat-transfer coefficient

From the temperature measurements, a surface heat-transfer coefficient of between 200 and 450 J/m$^2$ s °C could be obtained depending on loading and location in the pad. Since the temperature profile is expected to be quadratic, the higher values are used, as the true surface gradients are likely to be steeper than in a linear profile. A value of 450 J/m$^2$ s °C has been used in this case.

The pad thickness varies between a minimum of 0.0762 to a maximum of 0.2032 m. A 9 × 9 grid cannot reflect the abrupt changes in pad thickness in detail. Thus an average value of 0.127 has been used. The collar thickness has been taken to be twice the pad thickness.

## 2.2 Analysis of results

Figure 3 shows a graph of maximum pad surface temperature versus load. Another curve is plotted for the leading edge temperature versus load. Since the bearing supports a turbo-generator, an initial load of 6.5 MN represents the weight of the moving parts. An additional thrust is exerted by the water flow in the turbine which can be regulated to produce the different loading conditions. Both curves show a discrepancy in the range 0–3°C between the model and experiment. In numerical terms, this is considered satisfactory. The agreement between the experimental results and the numerical model is improved at the higher loadings. A maximum test load of 16 MN produced a maximum pad temperature of 90°C, compared to a value of 88.5°C for the present model

In Fig. 4, experimental and theoretical contour plots for temperature are presented at the pad–oil interface. It should be noted that the experimental contours for the pad surface have been interpolated and are likely to be lower than the true values. The shapes of the temperature contours are very similar. The position of the maximum temperature is also approximately the same—a small distance from the trailing edge (close to the 75–75 position). The inclusion of the conduction model for the pad is thought to be primarily responsible. If conduction is neglected, the position of the theoretical maximum temperature will be at the pad trailing edge as there is no path for the heat generated to escape from the oil film.

Figure 5a,b,c and d summarizes the theoretical characteristics for the pads. At a total bearing load of 16 MN, the minimum film thickness approaches (Fig. 5b) 30 $\mu$m. This necessitates an average surface roughness of less than 2 $\mu$m (**3, 4**). The ratio of maximum to minimum film thickness increases from 2 at 4 MN to 4 at 16 MN. The total oil film energy loss increases as the load is increased. The energy loss in the oil film may be divided into four components: conduction to the pad, conduction to the runner, convection of the heat in the oil and flow work (dissipation of mechanical energy).

 

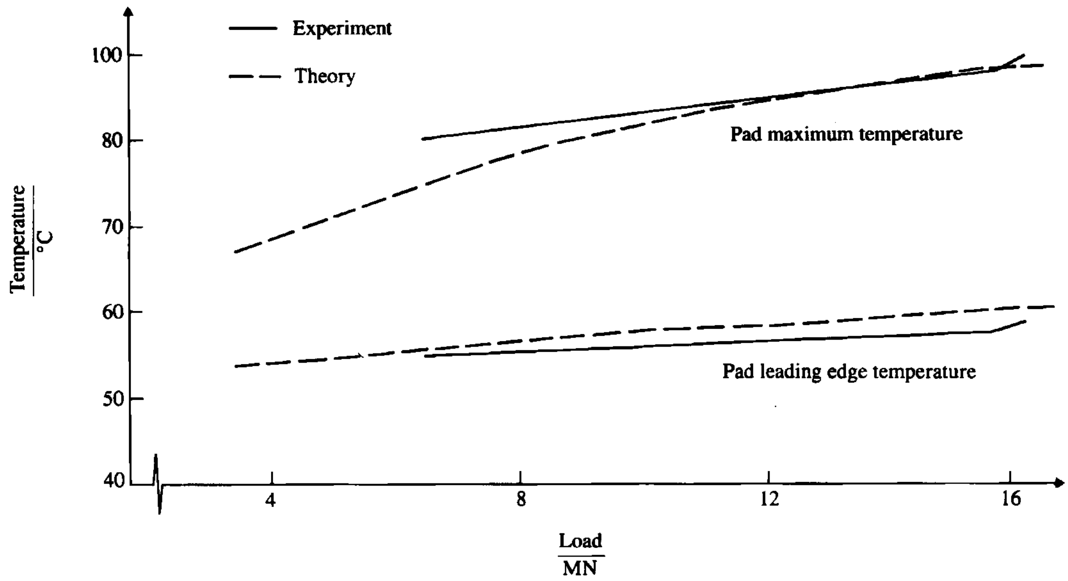


**Fig. 3** Pad temperature versus load (case 1)

The flow work term is very small (never more than 5 per cent).

The ratio of heat conducted to heat convected increases from 1 to 3 over the range 4–16 MN. In fact the amount of heat convected decreases. This casts doubts over the previous methods that lack a conduction model to both the pad and runner (**5–9**) and to their ability to predict correctly the oil film temperatures. Figure 5 shows a sizable decrease in the amount of oil entering the film leading edge as the load is increased. In contrast, the amount of heat convected shows only a small decrease (approximately 20 per cent). This is reflected as an increase in the oil film temperatures.

Figure 6a shows a contour map of theoretical film thickness values, non-dimensionalized with respect to the undistorted pivot film thickness ($h_{piv}$). All values in Fig. 6 relate to the 40 bar load case. The pad deflected shape is shown in Fig. 6e with the support positions superimposed. Contours of pressure (Fig. 6b) show a small cavitated area at the trailing edge. The position of $T_{max}$ closely corresponds with the position of minimum film thickness (Fig. 6a and c) both radially and circumferentially. The temperature distribution in the runner has a maximum value that falls directly above the maximum pad temperature (in the radial direction). The values of the maximum temperatures in the pad and collar are within 5°C. This suggests that the amount of conduction to the pad is very similar to that in the rotor. This is confirmed in Fig. 6.

Figure 7 shows three-dimensional surface contours of temperature in the pad, oil film and the runner when viewed from the same relative position. The oil film thickness variation has been omitted, and the pad width used as a film thickness in order to illustrate the temperature variations in the $z$ direction. Also shown is the deflected shape for the pad. The pad contours show a high intensity—reflecting a high temperature gradient—

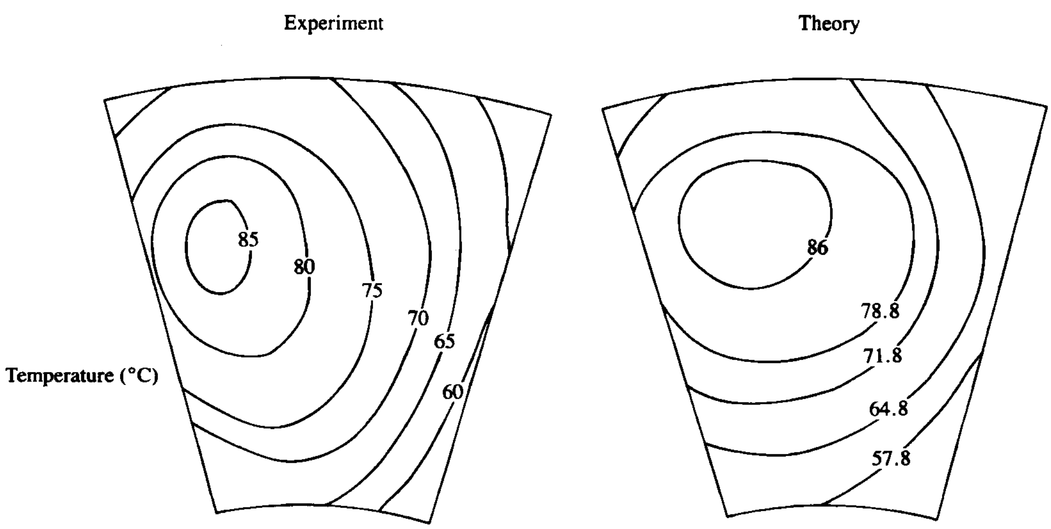


**Fig. 4** Experimental and theoretical temperature contours at pad–oil interface (case 1)

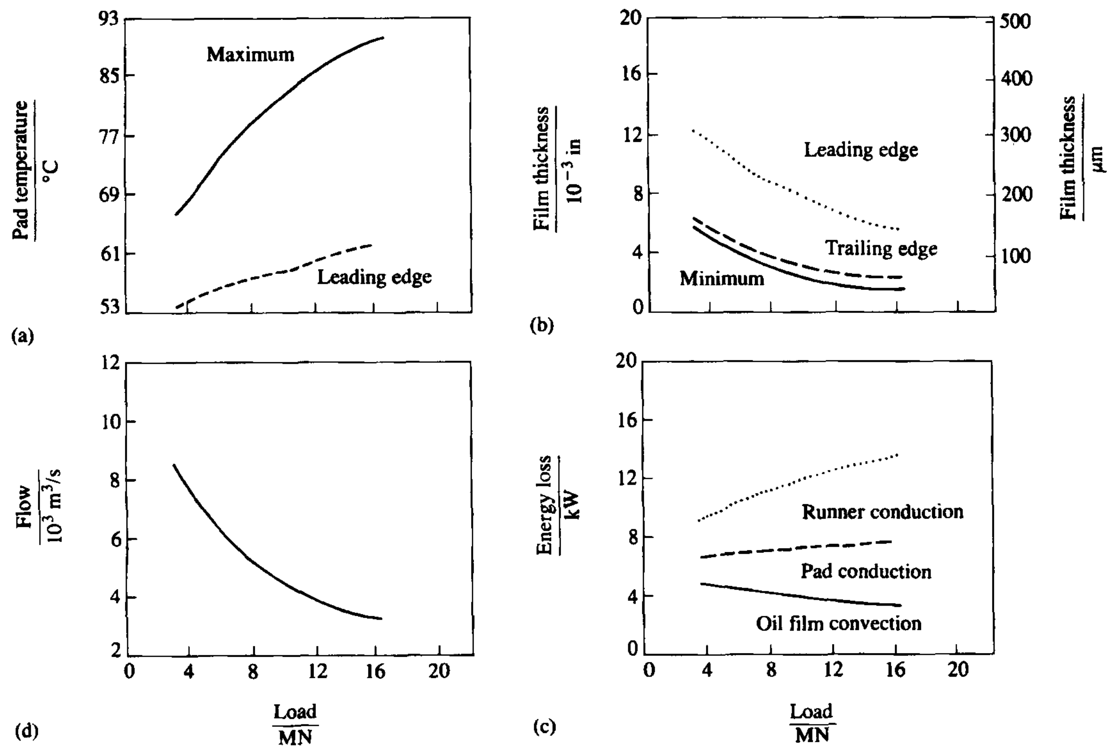


**Fig. 5** Pad theoretical characteristics (case 1)

in the $z$ direction compared with the lateral directions $r$, $\theta$. This indicates that conduction across the pad accounts for most of the heat conducted via the pad.

### 3 CASE 2—MEDIUM THRUST BEARING

Tests conducted at sea on the main propulsion thrust bearings of the destroyer *USS Barry* were reported by Elwell *et al.* (**10**). The main bearing specifications are listed in Table 2. The bearing consists of eight centrally pivoted pads. Temperature measurements were made at several locations in the pad including the pad centre. Measurements of oil groove temperatures were made using thermocouples of the same type as for the pad (copper–constantan). In addition film thickness measurements were carried out using two different systems—independent of each other. The first was a mutual inductance system which relies on the runner magnetic properties. The second is a capacitance system sensitive to the oil condition in the film. Overall accuracy of the film thickness measurements was estimated at $+5$ $\mu$m. In the present work, comparison is made with steady runs in smooth-water trials of *USS Barry* (as inaccuracies have been reported in rough-water measurements). Film thickness measurements were carried out for two shoes (pads). Comparison is limited to shoe number one (**10**) with an initial maximum crown of 10 $\mu$m.

The speed–load characteristic is given in Table 3. The bath temperatures varied between 96 and 109°F (35.6–42.8°C). For simplicity a value of 100.4°F (38°C) is taken as the steady bath temperature.

**Table 2** Bearing data for case 2

| | |
|---|---|
| Pad angle | 38.25 degrees |
| Inner radius ($R_i$) | 0.2096 m |
| Outer radius ($R_o$) | 0.3937 m |
| Number of pads | 8 |
| Pad thickness—minimum | 0.023 m |
| —maximum | 0.057 m |
| Pivot position | Centrally pivoted |
| Oil viscosity | 460 SUS at 100°F |
| | 121 SUS at 150°F |
| | 55.4 SUS at 210°F |
| Bath temperature | 38°C |
| Material | Steel |

#### 3.1 Numerical model

Since the pads are centrally pivoted, a regular grid has been used (see Fig. 8). For deflection the same boundary conditions apply as in case 1.

The surface heat-transfer coefficient values were obtained from thermocouple locations as described for case 1. The values are expected to be more accurate since temperature measurements were made at the pad–oil interface using thermocouple leads machined flush with the working surface. Figure 9 shows a correlation between the surface heat-transfer coefficient and rotational speed (hence the load). It appears that at low speeds (less than 10 rad/s) a negative surface heat transfer results. This is not possible and the coefficient values are expected to have a minimum positive value

**Table 3** Load–speed relationship for case 2

| Speed r/min | Unit loading lbf/in$^2$ |
|---|---|
| 100 | 50 |
| 200 | 205 |
| 300 | 495 |

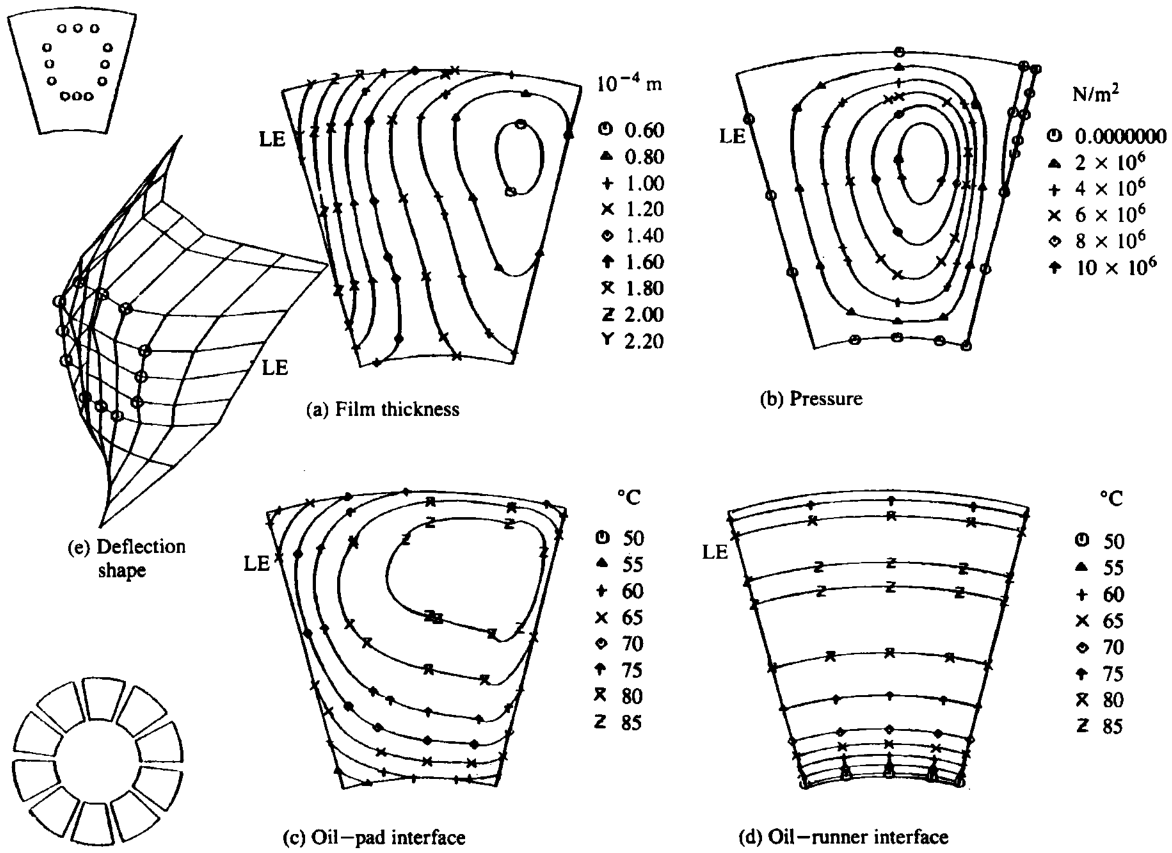


**Fig. 6** $p$, $T$, $h$ contours and deflection shape (case 1)

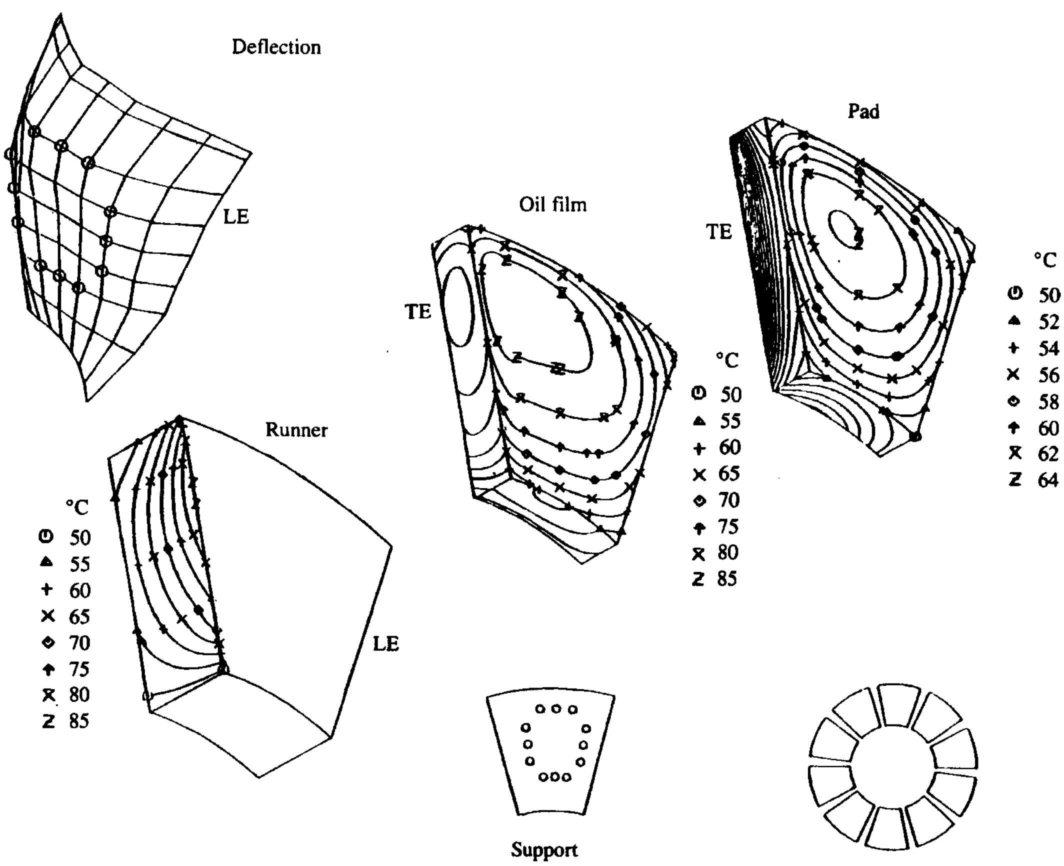


**Fig. 7** Contours of temperature in pad, runner and oil film (case 1)

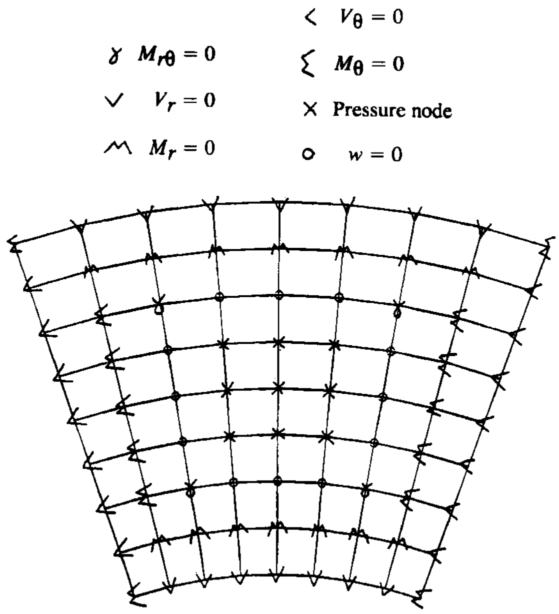


**Fig. 8** The grid and deflection boundary conditions (case 2)

representing free convection. However, since the region of interest lies above the speed of 10 rad/s, this correlation yields

$$\alpha = -162 + 16.2\Omega \qquad \text{for } \Omega > 10 \text{ rad/s}$$

The correlated values for $\alpha$ are obtained using the method outlined for case 1.

Elwell *et al.* (**10**) gave details of the pad thickness variations. Again for a 9 × 9 grid it was not possible to include them. The maximum thickness was 2.25 in (0.05715 m) and the minimum value was 0.775 in (0.019685 m). The average value was 1.5 in (0.0381 m) and was used as the pad thickness in the model. The

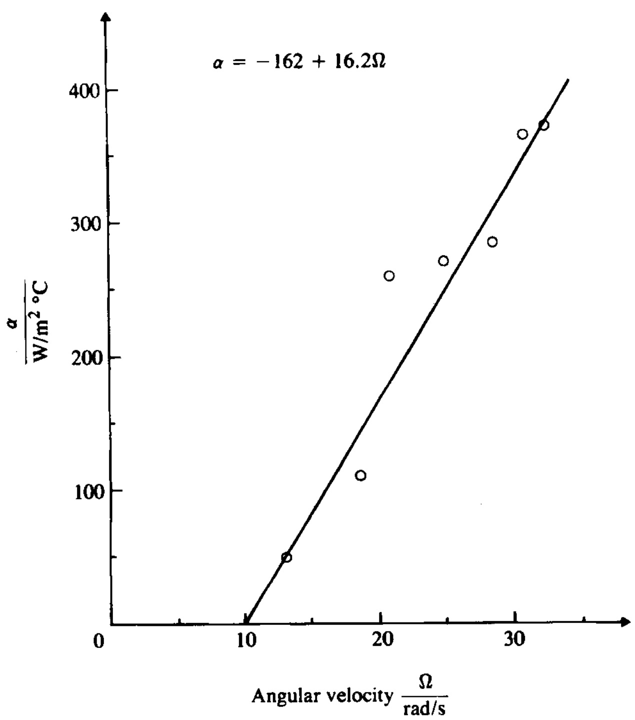


**Fig. 9** The variation of surface heat transfer with angular velocity (case 2)

runner thickness was assumed to be twice that of the pad.

### 3.2 Analysis of results

Figure 10 shows the film thickness variation with load at the pad centre. At 35 bar a difference of 5 $\mu$m exists between theory and measurement. As the load decreases, the gap widens to 15 $\mu$m. A difference of 5 $\mu$m is acceptable on the basis of the experimental errors reported. Thus a maximum film thickness error of 15 per cent results for the low load. The temperature at pad centre is also plotted versus the load (Fig. 10). A consistent gap of 7°F (approximately 4°C) is shown for the entire load range. Fortunately, the analysis renders a higher temperature than measured and is therefore conservative.

Contours of predicted pressures are shown in Fig. 11b. Film thickness contours are shown in Fig. 11a. The radial position of the minimum film thickness corresponds to the position of maximum temperature in both pad–oil and pad–runner interfaces (Fig. 11c and d). This is not the case when the circumferential position is considered. The hot core region on the pad surface (over 70°C) is circumferentially extended compared to the previous case. This may be partly due to the larger pad angle subtended. The film thickness pattern shows bending of the pad into a spherical shape, typical of a uniform plate with a constant temperature gradient across its thickness. Again this shows a marked contrast when compared to the film thickness pattern for the larger bearing in case 1. The deflection pattern (Fig. 11e) confirms this (also refer to Fig. 6a and e). Figure 12 shows three-dimensional surface temperature contours similar to those in Fig. 7. Two important differences may be observed. Firstly, the position of oil maximum temperature has moved radially outwards (that is near the outer radius). Secondly, that conduction along the pad (and runner) becomes as important as conduction through its thickness. This is reflected in a roughly equal spacing of contours along and across the pad. The vertical surface at the pad inner radius shows a hot spot at its centre. This is due to heat conducted along the pad from hotter regions (nearer the maximum temperature); the heat is eventually given to the cooler oil film at the inner radius—as well as to the back of the pad.

## 4 CASE 3—SMALL THRUST BEARING

In 1979 Neal (**11**) presented results of tests conducted on a 150 mm bearing. In 1981 (**12**), further results were presented for the same bearing. The main bearing specifications are given in Table 4. Different pad arrangements were used: three, four, six and eight (Fig. 13a).

The chamber oil temperature ($T_{\text{bath}}$) was measured at the positions indicated in Fig. 13a. The position of thermocouples within the pad are shown in Fig. 13b. The pads are assumed 'line' supported [as is the case for Glacier pads (**13**)]. It should be noted that the pads are not exactly sector shaped and details in Table 4 refer to the sector equivalent used for analysis. Temperature measurements were made at two positions in the runner using an air-cooled slip ring. The thermocouples, 2.5

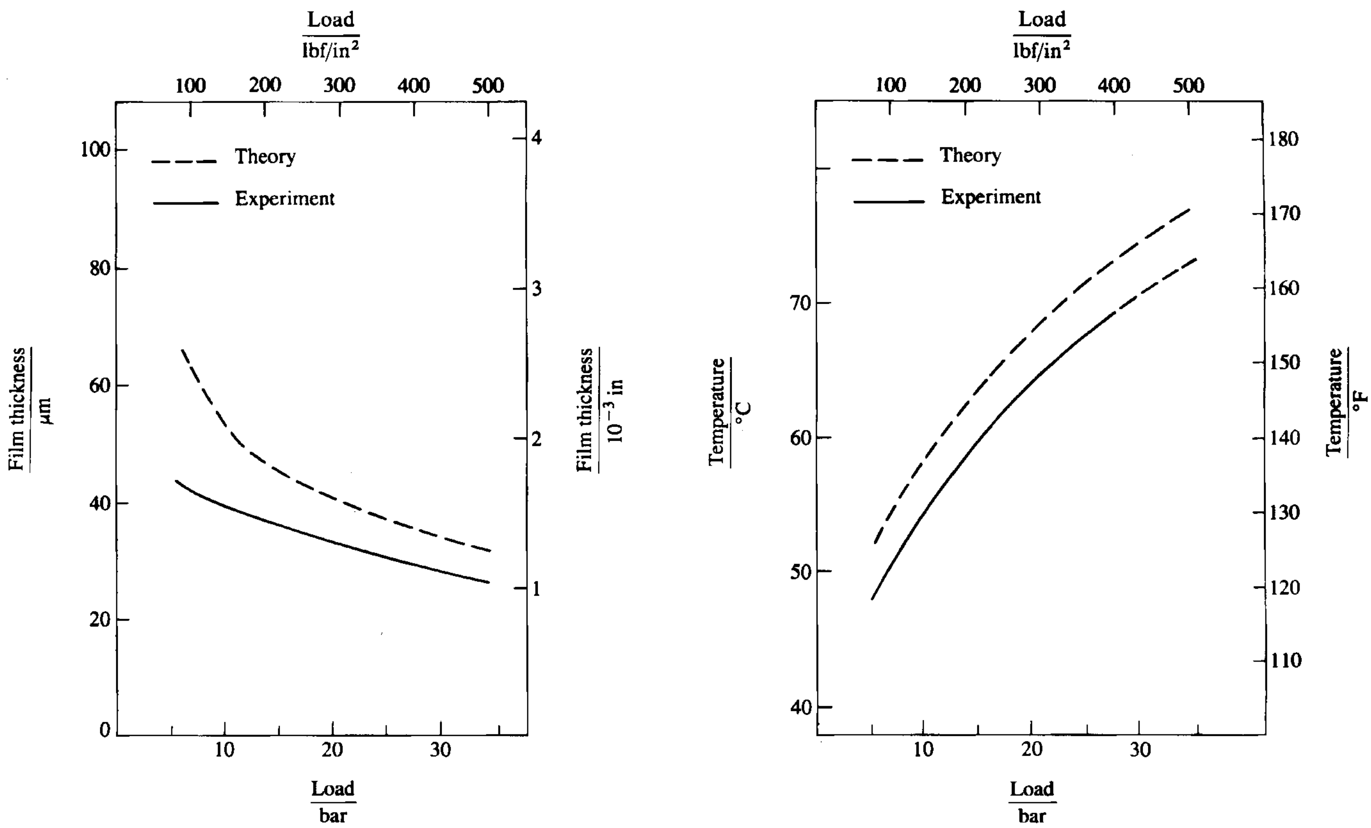


**Fig. 10** Temperature and film thickness versus load (case 2)

mm from the runner face, were located to correspond to the mid-radius of the bearing pads. The bearing operated in a flooded condition but the reverse face of the collar operated relatively free of oil by virtue of a radial seal at the runner outer diameter. Pad-to-pad temperature variation was a maximum of 3°C—an indication of small random errors involved (**11**). The oil supply rate was fixed; hence the bath temperature varied with load and speed. Tests were conducted at four different speeds. The oil bath temperature variation with load was given for the 3000 r/min case only. Thus, comparison will only be made at this speed.

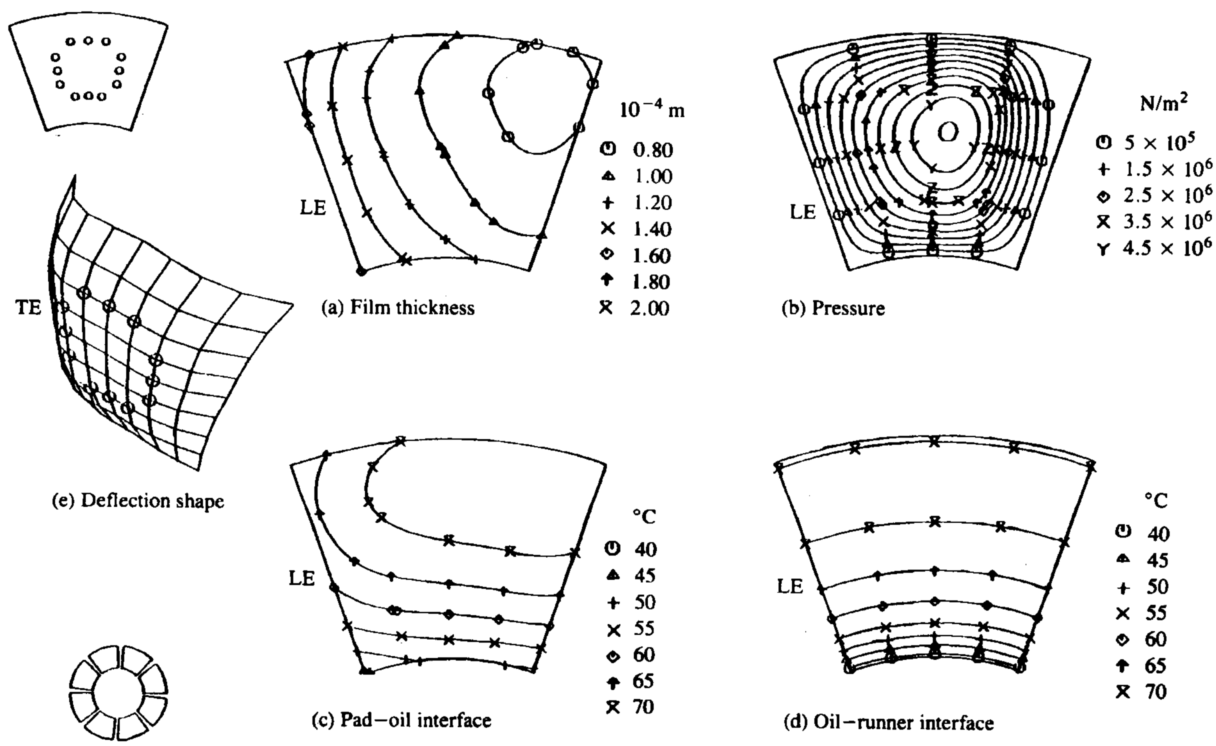


**Fig. 11** $p$, $T$, $h$ contours and deflection shape (case 2)

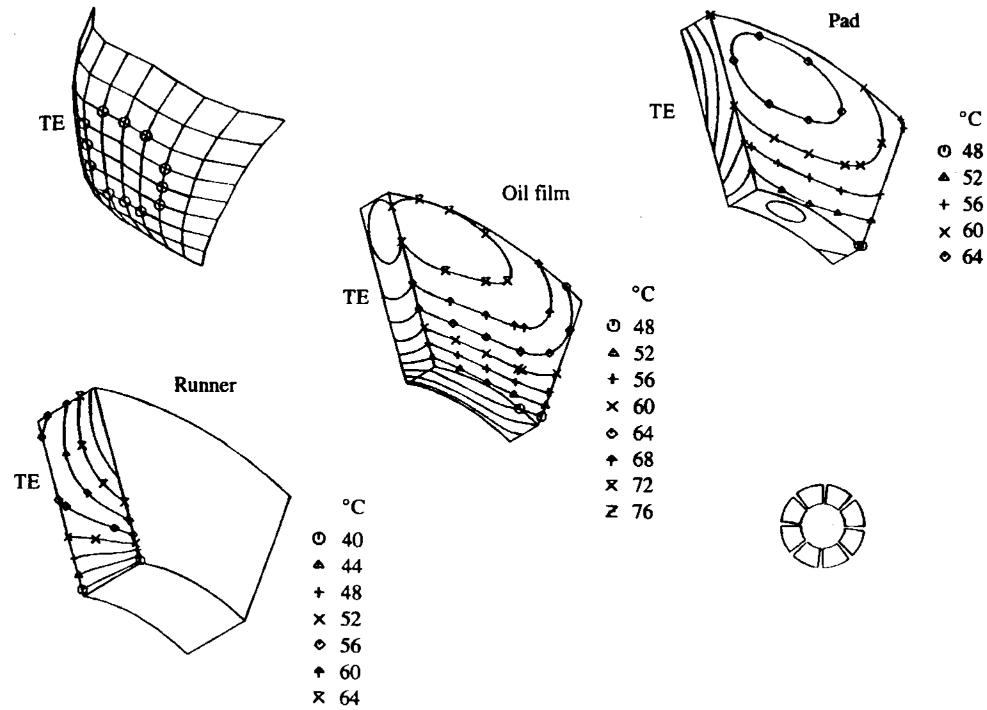


**Fig. 12** Contours of temperature in pad, oil film and runner (case 2)

### 4.1 Numerical model

In order to model a 'line' support an assumption has to be made regarding the width of 'line'. Figure 14 shows some alternative models. In Fig. 14a the support is shown as a series of fixed nodes along one line. Numerically this system is unstable since if the pressure forces are not exactly balanced a solution is not possible. This model cannot represent the true support since the 'line' is bound to have a finite width, however small. An alternative arrangement of support positions is shown in Fig. 14b. This leads to asymmetry, but has the advantage of stability for any pressure field distribution—not necessarily balanced about the line support. The complementary arrangement of nodes is shown in Fig. 14c. In Fig. 14d and e, two symmetrical arrangements are presented. Nodes $O_1$ and $O_2$ (and $O_3$ and $O_4$ in Fig. 14d) represent an increased stiffness in the tangential direction. Thus their position along the line support is important. In Fig. 14f a model is proposed which combines the virtues of all previous models. In essence two rows of nodes are chosen to represent the two edges of a line support of finite width. The width may be varied by varying the spacing between the nodes. On the other hand, the circumferential stiffness due to the support spans the whole length of the support. Figure 15 shows a plan of the pad with grid and node conditions shown.

The pivoting routine has also been adjusted to reflect a line support. Thus, tilting is carried out about the line support axis only (Fig. 15). The centre of pressure can lie at any point along the line support axis. The line support does not extend to the pad edges [as is the case with Glacier pads (**11**)]. The collar thickness is taken to be equal to three times the pad thickness (as given in specifications).

**Table 4** Bearing data for case 3

| | |
|---|---|
| Pad angle | 32 degrees |
| Inner radius ($R_i$) | 0.0395 m |
| Outer radius ($R_o$) | 0.0745 m |
| Number of pads | 3, 4, 6 and 8 |
| Pad thickness | 0.011 m |
| Pivot position | Line support (central pivot) |
| Angular velocity | 3000 r/min |
| Oil viscosity | 0.018 kg/m s at 122°F<br>0.01 kg/m s at 158°F<br>0.0045 kg/m s at 212°F |

| | Oil bath temperature °C | | |
|---|---|---|---|
| At | 3 pads | 6 pads | 8 pads |
| 5 kN | 59 | 61 | 63 |
| 10 kN | 62 | 63 | 65 |
| 15 kN | 63.5 | 65 | 66.5 |
| 20 kN | 65 | 66.5 | 68 |
| Pad material | | Steel | |

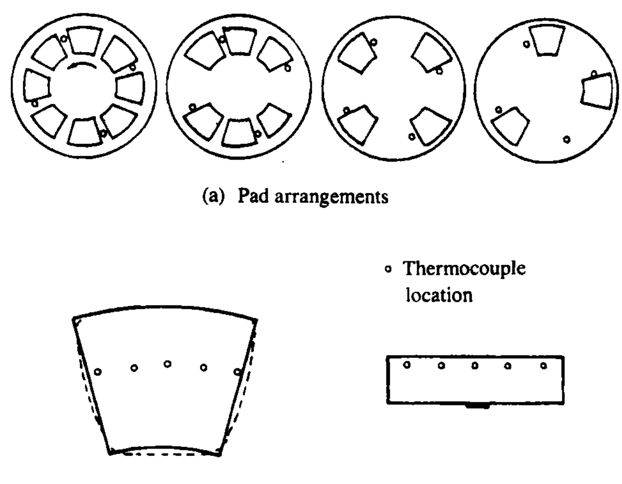


**Fig. 13** Pad arrangements and geometry (case 3)

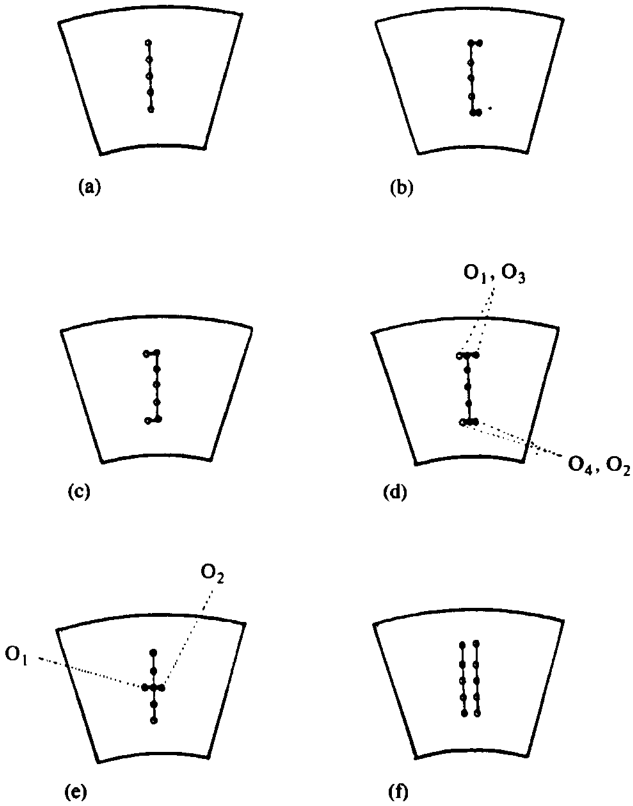


**Fig. 14** Models for a line support (case 3)

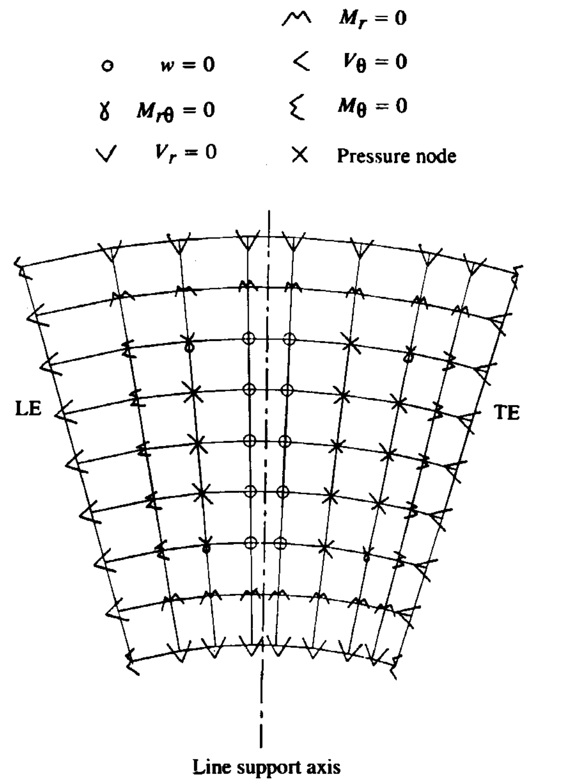


**Fig. 15** The grid and deflection boundary conditions (case 3)

No details were given concerning the variation of temperature across the pad. A value of 1000 J/m$^2$ s°C has been chosen to reflect good surface heat-transfer coefficient (compared to approximately 200 or 450 J/m$^2$ s °C in previous cases) for the back faces of the pad and collar side. The back of the runner has been described as relatively 'oil free'. Hence, a value of 10 J/m$^2$ s °C—two orders of magnitude lower—has been chosen to represent the surface heat-transfer coefficient for air.

### 4.2 Results and analysis

Figure 16 shows the maximum bearing temperature versus total bearing load for the three, six and eight pad arrangements. Since only five thermocouples were used at various tangential positions, along the same radius, the experimental values are expected to be equal to or lower than the actual maximum pad temperature. The difference between experimental temperature values for eight pads and three pads increases as the load is

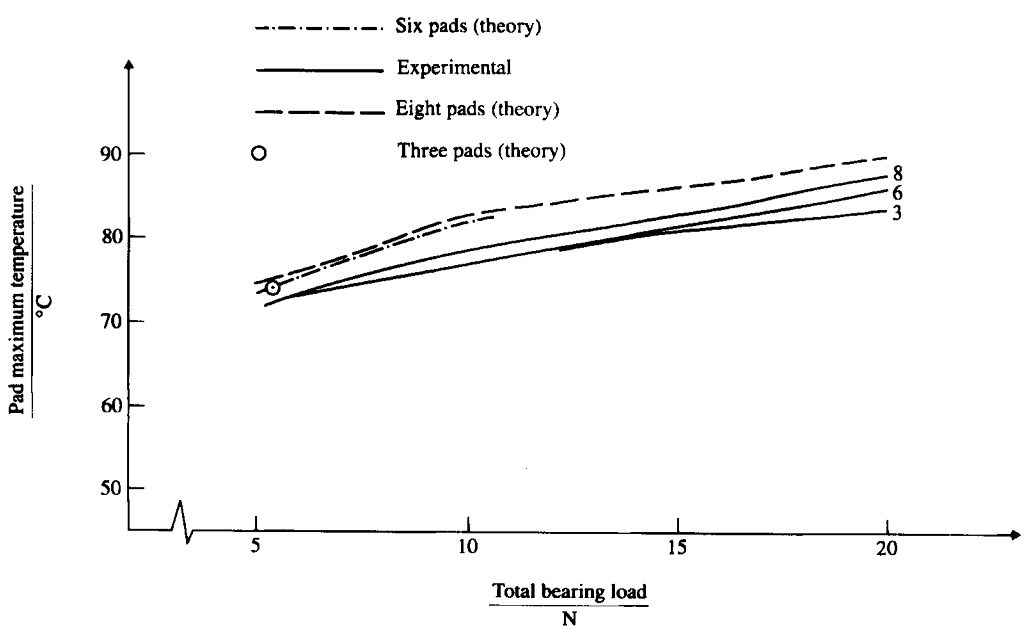


**Fig. 16** Pad maximum temperature versus total bearing load (case 3)

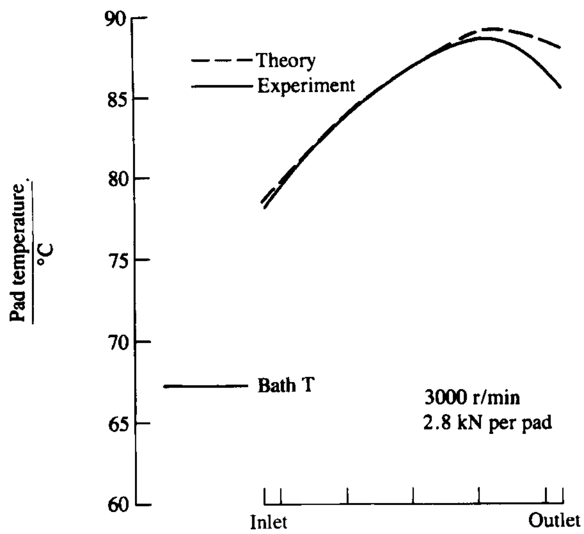


**Fig. 17** Pad circumferential temperature distribution

increased. The difference at 20 kN is 4.5°C. The difference between the numerical model temperatures and measured values for the eight pad case does not exceed 5°C and narrows down to 2°C at 20 kN. Various numerical values for three and six pads are also shown.

Figure 17 shows the circumferential temperature distributions for $r = 0.83\ r_0$ (where the thermocouples were located). A maximum variation of 2°C is found at pad outlet. The difference, for the maximum temperature, does not exceed 0.5°C. The temperature gradients at inlet and outlet (see Fig. 17) are steeper for the experimental values. This indicates that the heat-transfer coefficients—at least for the side faces—are higher than the values used. Nevertheless the values used are satisfactory for prediction purposes and are thought to be close to the actual values.

In Fig. 18 the various energy components (conduction to rotor, conduction to pad, and convection) in the oil film are shown for the three and eight pad cases versus total bearing load. The energy refers to that for a single pad oil film. Three observations can be made. Firstly, the total energy generated per pad is higher for the three pad arrangement. This is expected since only three pads carry the same load carried by eight pads in the second arrangement. The total energy generated for the whole bearing (for all pad oil films) is smaller in the three pad case, indicating a smaller power loss. The churning power loss in the inter-pad cavities is not evaluated, but is expected to be larger for the three pad case—diminishing the advantage of the three pad arrangement. A similar trend is verified experimentally (**12**). For the eight pad arrangement, at a load of 20 kN, the total power loss per pad is found to be 232 W compared to a predicted value of 180 W. This represents a difference of 22 per cent. The second observation concerns the proportion of total heat convected to total heat conducted. In both cases conduction plays a critical role; the proportion of heat convected to heat conducted being 1 and 0.5 for the eight and three pad cases respectively. The third observation concerns the role of the runner in conducting away heat. The runner conduction for the three pad case is greater than both convection and pad conduction combined. This is due to the large inter-pad cavities serving to absorb the energy conducted to the runner below the pads. This effect is diminished in the eight pad arrangement, since less area is covered by the cavities compared to the area covered by oil film below the pads. All three observations are found in Neal's recent experimental investigation (**12**).

Figure 19 shows results for the eight pad arrangement at a load of 19 kN. The film thickness contours (Fig. 19a) show a predominantly cylindrical deflection

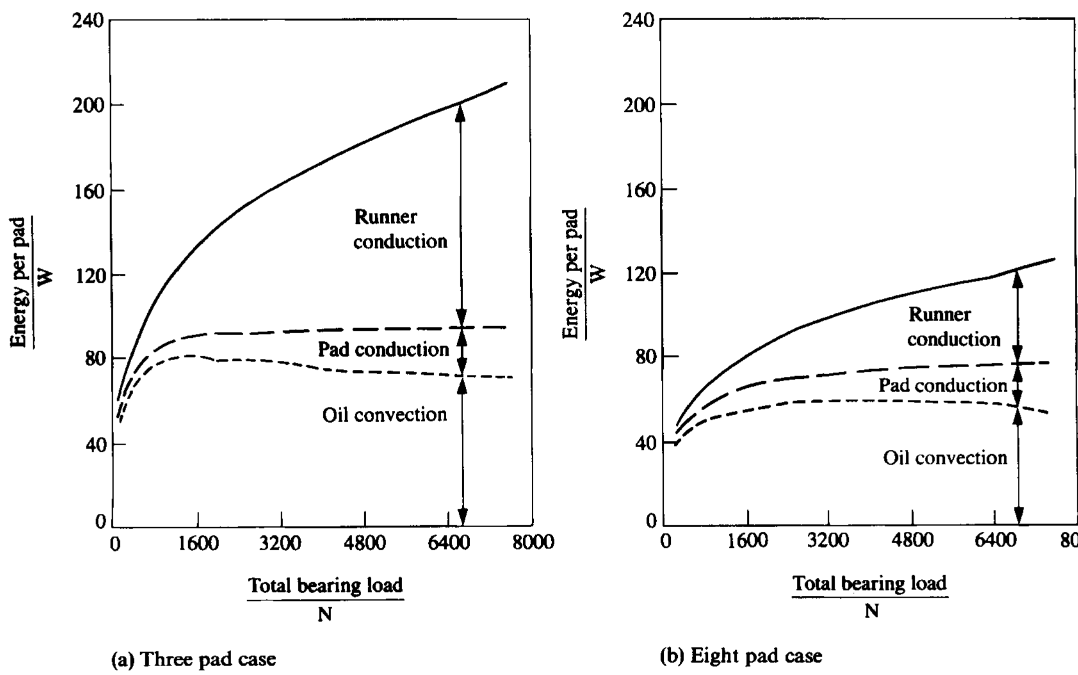


**Fig. 18** Energy conduction and convection versus total bearing load for the oil film (theory)

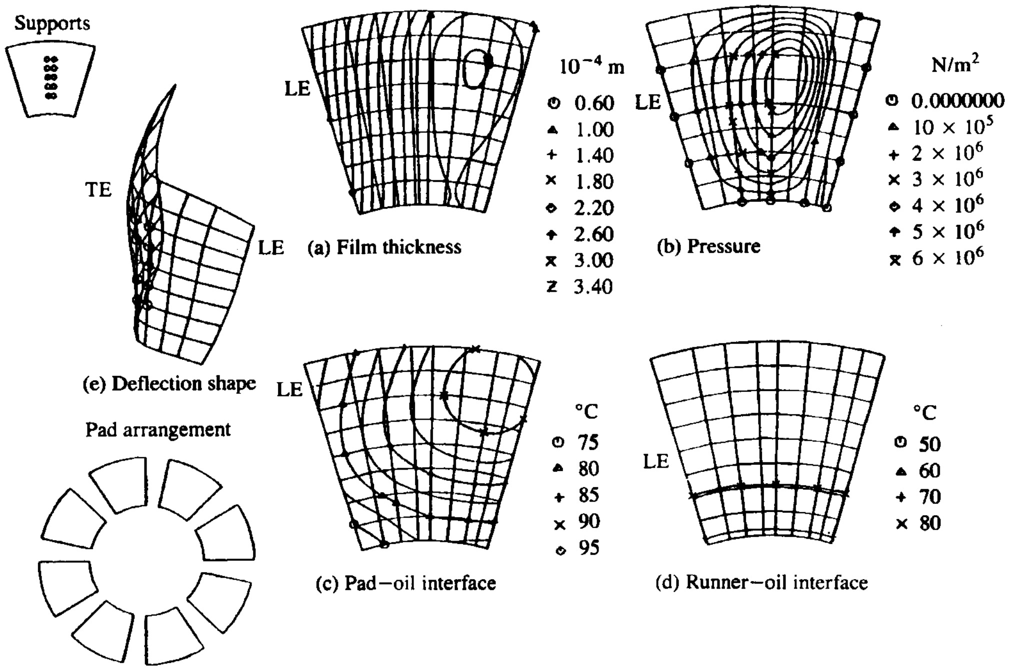


**Fig. 19** $p$, $T$, $h$ contours and deflection shape (case 3): eight pad arrangement

pattern (rather than spherical as in the previous two). This is reflected in the deflected shape (Fig. 19e). The minimum film thickness positions, as well as the maximum pad temperature positions, have been shifted towards the outer radius compared to previous pad sizes. Figure 20 shows three-dimensional surface contouring results for temperature as well as the deflection shape. For the pad, the density of temperature contours in the $r$, $\theta$ plane is similar to that in the $r$, $z$ plane. This shows that temperature gradients along and across the pad are similar.

## 5 CONCLUSIONS

The comparisons between predicted and measured performance of three sizes of bearing have demonstrated

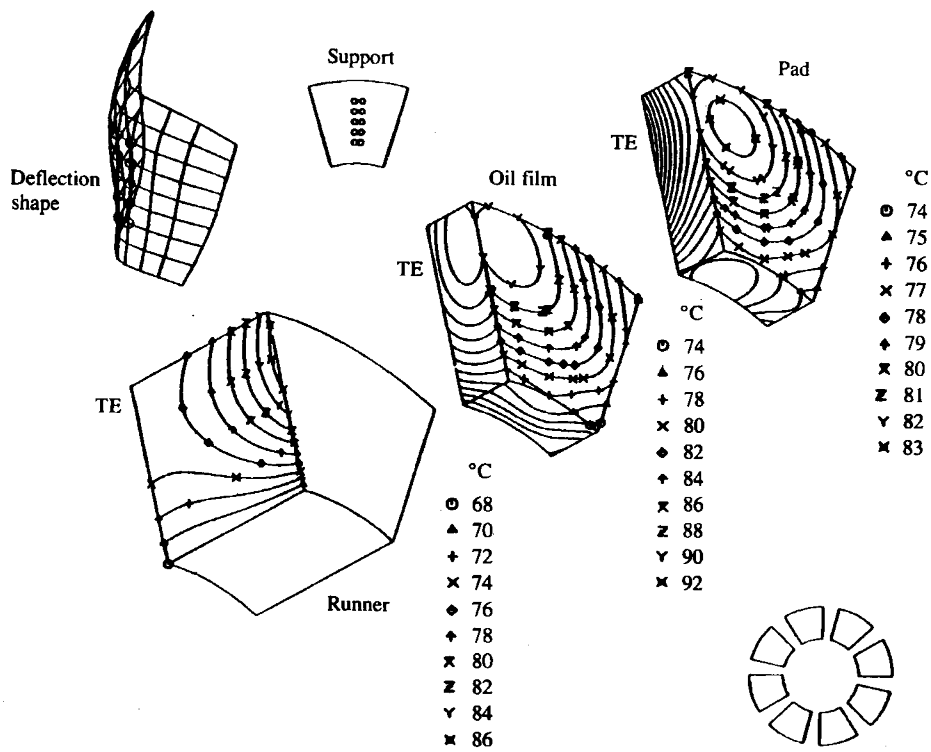


**Fig. 20** Contours of temperature in pad, runner and oil film (case 3): eight pad arrangement

the reliability of the proposed theoretical model for tilting pad thrust bearing analysis. Good agreement was obtained over a wide range of bearing size for temperatures in the pads. In the first test case (large bearing), the surface temperature distribution was successfully predicted at the pad–oil interface. In the third test case (small bearing), the pad circumferential temperature profile corresponded closely with the experimental measurements. In the second case (medium size bearing), broad agreement was obtained for both temperatures and film thicknesses.

Concerning the numerical modelling technique, the flexibility of the mesh system was demonstrated by its ability to accommodate the various pad support shapes (ring and line supports) for offset and centrally pivoted pads.

## ACKNOWLEDGEMENT

Financial support for this work was provided by the Science and Engineering Research Council.

## REFERENCES

1 Performance of Rocky Ridge thrust bearing, Vickers Limited, Michell Bearings, Report 74341, 1971.

2 **Timoshenko, S. P.** and **Woinowsky-Krieger, S.** *Theory of plates and shells*, 1959 (McGraw-Hill, New York).

3 **Cameron, A.** The surface roughness of bearing surfaces and its relation to oil film thickness at breakdown. *Proc. Instn Mech. Engrs.*, 1949, **161**, 73.

4 **Capitao, J. W., Gregory, R. S.** and **Whitford, R. P.** Effects of high operating speeds on tilting pad thrust bearing performance. *Trans. ASME, J. Lubric. Tech.*, 1976, **98**, 73–80.

5 **Castelli, V.** and **Malanoski, S. B.** Method for the solution of lubrication problems with temperature and elasticity effects: application to sector, tilting pad bearings *Trans. ASME, J. Lubric. Tech.*, 1969 **91**, 634–640.

6 **Ezzat, H. A.** and **Rohde, S. M.** A study of the thermohydrodynamic performance of finite slider bearings. *Trans. ASME*, 1973, Ser. F, **95**, 298–307.

7 **Huebner, K. H.** A three-dimensional thermohydrodynamic analysis of sector shaped thrust bearings. *Trans. ASLE*, 1974, **17**, 62–73.

8 **Sternlicht, B., Carter, G. K.** and **Arvas, E. B.** Adiabatic analysis of elastic centrally-pivoted, sector, thrust bearing pads. *J. Appl. Mech.*, 1961, **28**, 179–187.

9 **Ettles, C.** Development of a generalised computer analysis for sector shaped tilting pad thrust bearings. *Trans. ASLE*. 1975, **19**, 152.

10 **Elwell, R. C., Gustafson, R. E.** and **Reid, J. C.** Performance of centrally pivoted, sector, thrust bearing pad in sea trials aboard *U.S.S. Barry*. ASME paper 63-VA-124, 1963.

11 **Neal, P. B.** Some factors influencing the operating temperature of pad thrust bearings. Proceedings of sixth Leeds–Lyon symposium on Tribology, *Thermal effects in tribology* (Eds D. Dowson, C. M. Taylor, M. Goder and D. Berthe), 1979, pp. 137–142 (Mechanical Engineering Publications, London).

12 **Neal, P. B.** Heat transfer in pad thrust bearings. *Proc. Instn. Mech. Engrs.*, 1982, **196**, 217–228.

13 *Designer's Handbook 5*, Glacier Metal Company.